JOURNAL OF AEROSOL MEDICINE AND PULMONARY DRUG DELIVERY
Volume 24, Number 2, 2011

Pp. 103–118
DOI: 10.1089/jamp.2010.0849

Improving the Lung Delivery of Nasally Administered Aerosols During Noninvasive Ventilation—An Application of Enhanced Condensational Growth (ECG)

P. Worth Longest, Ph.D.,[1,2] Geng Tian, M.S.,[1] and Michael Hindle, Ph.D.[2]

Abstract

Background: Aerosol drug delivery during noninvasive ventilation (NIV) is known to be inefficient due to high depositional losses. To improve drug delivery efficiency, the concept of enhanced condensational growth (ECG) was recently proposed in which a submicrometer or nanoaerosol reduces extrathoracic deposition and subsequent droplet size increase promotes lung retention. The objective of this study was to provide proof-of-concept that the ECG approach could improve lung delivery of nasally administered aerosols under conditions consistent with NIV.
Methods: Aerosol deposition and size increase were evaluated in an adult nose–mouth–throat (NMT) replica geometry using both *in vitro* experiments and CFD simulations. For the ECG delivery approach, separate streams of a submicrometer aerosol and warm (39°C) saturated air were generated and delivered to the right and left nostril inlets, respectively. A control case was also considered in which an aerosol with a mass median aerodynamic diameter (MMAD) of 4.67 μm was delivered to the model.
Results: *In vitro* experiments showed that the ECG approach significantly reduced the drug deposition fraction in the NMT geometry compared with the control case [14.8 (1.83)%—ECG vs. 72.6 (3.7)%—control]. Aerosol size increased from an initial MMAD of 900 nm to a size of approximately 2 μm at the exit of the NMT geometry. Results of the CFD model were generally in good agreement with the experimental findings. Based on CFD predictions, increasing the delivery temperature of the aerosol stream from 21 to 35°C under ECG conditions further reduced the total NMT drug deposition to 5% and maintained aerosol growth by ECG to approximately 2 μm.
Conclusions: Application of the ECG approach may significantly improve the delivery of pharmaceutical aerosols during NIV and may open the door for using the nasal route to routinely deliver pulmonary medications.

Key words: respiratory drug delivery, nanoaerosols, hygroscopic droplet growth, high flow therapy, noninvasive positive pressure ventilation, adult nasal–mouth–throat (NMT) model, *in vitro* deposition experiments, CFD modeling

Introduction

Noninvasive ventilation (NIV) is currently a form of standard care for patients suffering from respiratory insufficiency, sleep apnea, chronic obstructive pulmonary disease (COPD), and more severe acute and chronic respiratory failure. For patients requiring high levels of NIV comparable to the inspiratory flow rate, current options are noninvasive positive pressure ventilation (NPPV)[1] and high flow therapy (HFT).[2] With NPPV, a mask or other interface supplies positive pressure flow to the nose and mouth.[3] Extensive reviews have indicated the benefits of NPPV in adults[1,4–6] and children.[7] In HFT, air or blended oxygen is preconditioned with heat and water vapor (humidity) to allow continuous delivery through a nasal cannula up to flow rates of 40 L/min.[2] This approach is currently being applied

[1]Department of Mechanical Engineering, and [2]Department of Pharmaceutics, Virginia Commonwealth University, Richmond, Virginia.

to treat pulmonary edema, COPD, bronchiectasis, and acute respiratory distress syndrome (postintubation).[2] In adults, HFT has been shown to significantly increase exercise tolerance and reduce dyspnea,[8,9] as well as to significantly improve quality of life scores.[10] Based on these clinical successes, the use of NIV is currently increasing in both critical care units[11–13] and home care settings.[14]

Patients receiving NIV typically have underlying respiratory and systemic conditions that could be effectively treated with pharmaceutical aerosols.[3,15] Aerosol delivery during NIV can be very convenient for patients, especially when high doses and relatively long nebulization times are required or for short-acting medicines that require frequent administration.[16] Historically, bronchodilators were routinely given during NPPV;[17] however, a reduction in usage followed the observation that drug delivery was inefficient due to high aerosol losses.[18] Based on more recent studies, patients with asthma and COPD who received bronchodilators delivered through a NPPV system showed significant improvement.[19–21] Infants receiving invasive and noninvasive ventilation also showed a positive response to bronchodilators.[22] However, both *in vivo* and *in vitro* studies have illustrated that high aerosol losses occur in NIV systems, resulting in very low delivery rates, which are on the order of <1–10% in adults and children.[3,22] The success of bronchodilator therapy despite very low delivery rates occurs because of a wide therapeutic window with these types of drugs coupled with low side effects. However, adverse side effects of bronchodilators and ipratropium bromide depositing on the face and in the eyes during NIV have recently been reported.[23,24]

Very low delivery rates of aerosols during NIV occur because of depositional losses in the aerosol generator, connective tubing, and patient interface, as well as in the narrow and thin nasal passages. Previous studies have focused primarily on evaluating aerosol deposition in NPPV systems. *In vitro* studies with NPPV indicate that deposition losses within the delivery system are approximately 90% or greater, resulting in only 10% of the aerosol reaching the inlet of the extrathoracic airways.[3,25,26] Similar *in vivo* NPPV studies report delivery to the face mask on the order of 1–6%.[19] The study of Sangwan et al.[27] considered facial aerosol deposition with a NPPV system and found that it was comparable to or greater than the inhaled dose. The only available study on aerosol deposition in a HFT system was performed by Bhashyam et al.,[16] who considered delivery output from a nasal cannula operating at 3 L/min intended for infant respiratory support. Total drug output ranged from approximately 8 to 25% as a function of cannula size. Surprisingly, no previous studies report on nasal or extrathoracic losses during NIV aerosol delivery. Based on predictions for nasal deposition with standard aerosol sizes of 2–7 μm,[28,29] the nasal airways are likely to further reduce the lung dose from NIV systems by an additional 40 to 99%. Mesh nebulizers that are synchronized to generate aerosol during inspiratory flow have been shown to improve drug delivery during invasive mechanical ventilation.[15,30] However, significant deposition of these relatively large-sized medical aerosols in the nasal passages will be a problem for NIV applications.

As described, bronchodilators and corticosteroids delivered during NIV may be clinically effective, but deposition efficiencies are very low and side effects are prevalent. A recent review of orally inhaled products by Borgstrom et al.[31] indicated that high drug losses in the inhaler and extrathoracic airways correlated directly with high variability in lung delivery. It is reasonable that high delivery system and nasal losses during NIV will also produce high variability in the amount of drug aerosol reaching the lungs. Based on previously observed low lung deposition rates coupled with high dose variability, existing systems used for delivering aerosols during NIV may not be appropriate for many next-generation medications. Moreover, these next-generation inhaled medications may fail clinically because of a lack of knowledge regarding the actual dose reaching the patient. Examples of inhaled medications that may benefit patients receiving NIV include prostanoids [for acute respiratory distress syndrome (ARDS), pneumonia, and pulmonary hypertension], antibiotics (for lung infections), surfactants (for neonatal respiratory distress syndrome and ARDS) and mucolytics (for cystic fibrosis).[15] Compared with existing therapies, most of these proposed inhaled medicines have a narrow therapeutic range, serious potential side effects, and are more expensive. As a result, for these medicines to be successfully administered to NIV patients, efficient and reproducible lung delivery is essential.

To improve drug delivery efficiency for orally inhaled pharmaceutical aerosols, the concept of enhanced condensational growth (ECG) was recently proposed.[32–35] In this approach, separate streams of submicrometer aerosol and saturated or supersaturated warm air are delivered to the mouth–throat (MT). Mixing of these two streams in the upper airways or cooling from the airway walls results in supersaturated conditions and condensational growth of the aerosol at a controlled rate. Due to the initial submicrometer size, the aerosol has negligible deposition in the MT and extrathoracic airways resulting in high lung delivery rates. Condensational growth as the aerosol enters the lungs increases droplet sizes to approximately 2 μm or greater with the intent of fostering lung deposition and preventing exhalation of the aerosol. Previous studies have suggested that hygroscopic growth should be taken into account in determining the lung deposition of drug aerosols[36–38] and can be used for the formation of an aerosol.[36,39] However, the delivery of relatively small particles or droplets with the intent of reducing extrathoracic deposition followed by intentional and controlled growth to ensure lung retention is unique to the ECG approach.

Longest et al.[34] recently demonstrated the ECG delivery concept in a simple tubular model and found that size increases from approximately 500 nm to 3 μm were possible under typical inhalation conditions. Longest and Hindle[32] developed a computational fluid dynamics (CFD) model that accurately simulated aerosol size increase compared with experimental results. Hindle and Longest[35] considered a model of the MT and tracheobronchial (TB) respiratory airways through generation G5 and found that the ECG approach greatly reduced upper airway losses (5% ECG vs. 70% control) and resulted in significant droplet size increase (approximately 500 nm to 3 μm). The CFD model was also found to accurately match the experimental deposition results in the MT–TB geometry.

Based on preliminary findings for orally inhaled medicines, ECG is proposed in the current study as a method to significantly improve the lung delivery of nasally administered

aerosols during NIV. Submicrometer aerosols are expected to significantly reduce depositional losses in the delivery lines and patient interfaces of NIV systems.[40] Moreover, submicrometer aerosols are known to have very low depositional losses in the nasal airways.[28,41,42] One possible approach for applying the ECG concept to improve aerosol delivery during HFT is proposed in the current study in which a submicrometer aerosol is provided to one nostril at slightly subsaturated conditions. A humidified airstream that is saturated with water vapor is delivered to the other nostril with a temperature a few degrees above *in vivo* wall conditions. The nasal septum physically separates the two streams allowing for the submicrometer aerosol to remain small and not deposit in the torturous nasal passages. Upon entry into the nasopharynx, the aerosol and now supersaturated airstream are combined resulting in condensational growth as the mixture continues downstream and enters the lungs. It is anticipated that this approach can reduce aerosol deposition and loss from the current standard of 90% to 10% or less. As a result, the delivery of conventional inhaled medications or next generation inhaled drugs during NIV can potentially become more effective with less variability and decreased side effects, producing a net reduction of overall expense and improved patient outcomes.

The objective of this study is to provide initial proof of concept that the ECG approach can be used to improve the lung delivery of nasally administered aerosols. As an initial case study, aerosol delivery through an adult nose–mouth–throat (NMT) model will be evaluated under flow conditions similar to HFT, which has not previously been considered. Aerosol deposition and size will be assessed for a standard nebulized aerosol and for ECG delivery conditions. The airway model considered includes the nasal passages through a portion of the trachea. *In vitro* experiments and CFD simulations will be used to investigate the flow field dynamics, aerosol size change, deposition, and outlet aerosol size conditions for the NMT geometry. Once tested in comparison with the *in vitro* results, the CFD model will also be used to investigate the effects of additional inlet temperatures and airway wall conditions on the performance of ECG delivery.

Methods

NMT geometry

To assess aerosol delivery during NIV, a representative model of the NMT extending through a portion of the trachea was constructed, as shown in Figure 1. The nasal geometry was based on the MRI data set originally reported in the study of Guilmette[43] for an adult male and subsequently used in a number of *in vitro* experiments[29,44–46] and CFD simulations.[41,47,48] The surface area to volume ratio of this model is approximately 1, which is consistent with population mean values for healthy adults.[49–51] Further details related to the construction of this model can be found in the previous studies of Xi and Longest.[41,42] The nasal cavity model was connected to the realistic MT geometry described by Xi and Longest.[52] Critical dimensions of the MT geometry are a glottal cross-sectional area of 0.87 cm^2 and a tracheal cross-sectional area of 2.0 cm^2, which are consistent with commonly used values for adults.[52] The nasal and MT models were joined in the nasopharynx region based on anatomical images and an existing NMT geometry.[42]

The NMT surface model shown in Figure 1 was used to construct a hollow geometry for the *in vitro* experiments. The hollow model was built using an in-house Viper SLA machine (3D Systems, Valencia, CA), which uses a 100-mW solid-state laser to selectively harden clear Accura 60 plastic resin. For the NMT geometry, the build layer thickness was 0.15 mm and the laser spot diameter was 0.25 mm. In this preliminary study, deposition with a cannula interface positioned in the nose was not assessed. Instead, inlets were added to each nostril with a diameter of approximately 7 mm, which is consistent with the size of adult cannula nasal prongs. Using a similar diameter provides an inlet Reynolds number and turbulence profile that is consistent with cannula delivered flow. However, the effect of the cannula jet on local deposition in the nasal vestibule is not directly assessed in this study.

The NMT surface model was also used to construct a computational mesh that was identical to the experimental geometry. For cases in which the CFD results were compared directly to the *in vitro* data, the 7-mm inlet extensions were included in the model. However, additional CFD simulations were also conducted in the absence of the inlet extensions.

Experimental overview

Separate streams of aerosol and humidified air were generated and delivered to the right and left nostril inlets, respectively. The outlet of the NMT was connected directly to the inlet of the Andersen cascade impactor (ACI, Graseby-Andersen Inc, Smyrna, GA) operating at a flow rate of 30 L/min, which determined the particle size distribution of the aerosol after passage through the nasal airway model. A modified compressed air-driven humidifier system (Vapotherm 2000i, Stevensville, MD) was employed to generate saturated heated air that entered the airway model geometry at a flow rate of 20 L/min. The temperature of the humidified air at the nasal inlet was 25°C for the control and 39°C for ECG. The aerosol was generated at room temperature and delivered to the nasal model using a 7-mm diameter tube. To maintain the NMT geometry and impactor temperature, they were housed in a controlled environment chamber (Espec Environmental Cabinet, Grand Rapids, MI) and maintained at 37°C and 99% relative humidity (RH). The nasal model was preconditioned with supersaturated air and allowed to equilibrate in the chamber to ensure that the airway walls within the model were wetted prior to each experiment. Temperature and relative humidity measurements were made using a HUMICAP Handheld Meter (HMP75, Vaisala, Helsinki, Finland). Details related to aerosol generation, deposition, and size assessments are provided below.

Experimental aerosol generation

For the ECG experiment, nano-sized aqueous-based drug aerosols were generated using a small particle aerosol generator (SPAG- 6000, ICN Pharmaceuticals, Costa Mesa, CA). Albuterol sulfate solutions were nebulized to produce an aerosol with an initial mean (SD) measured size of 900 (32.7) nm and a geometric standard deviation (GSD) of 1.82. The aerosol was generated using a 0.5% albuterol sulfate in water

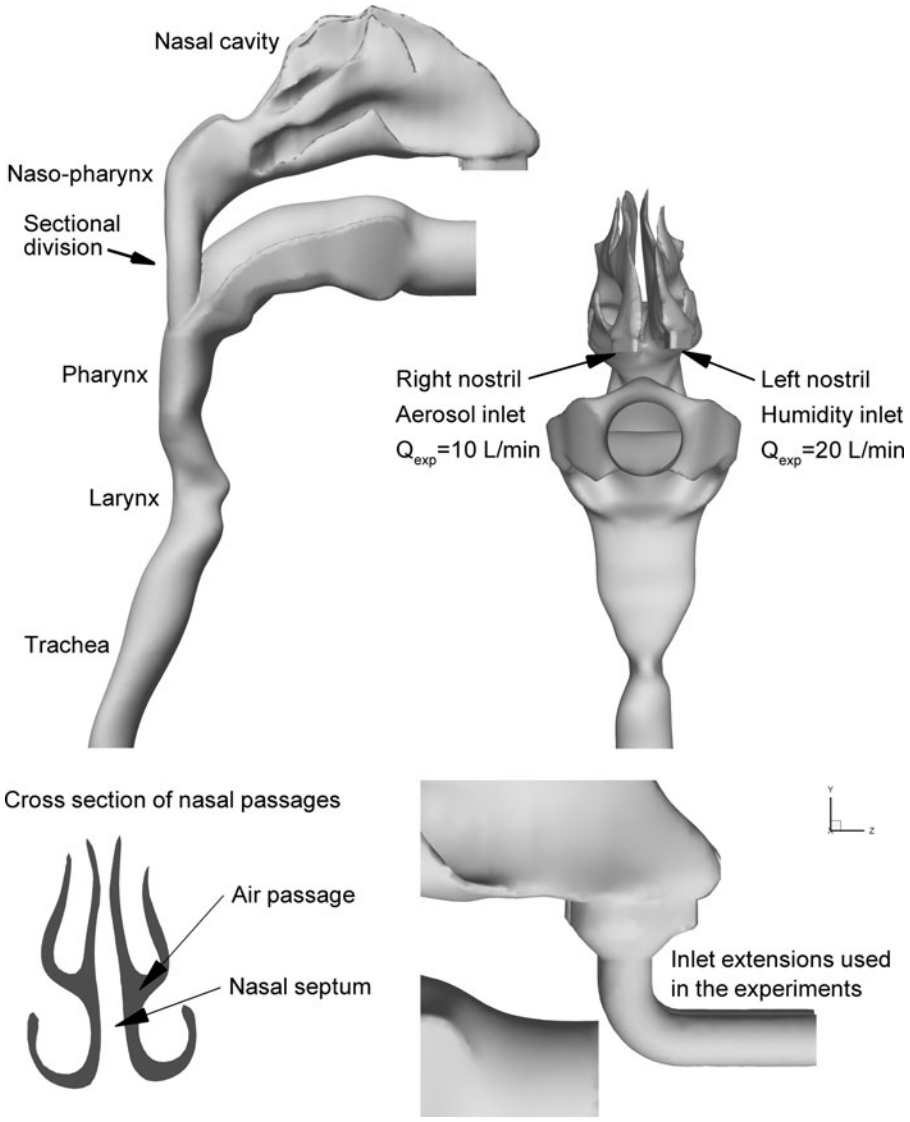

FIG. 1. Surface model of the nose, mouth, and throat (NMT) geometry extending through approximately midway the trachea. For all cases considered, the aerosol was delivered to the right nostril and the humidity was delivered to the left nostril. Flow rates used in the experiments (Q_{exp}) are shown for each nostril. For Cases 1 and 2, inlet extensions were included in the experimental and CFD models to deliver the aerosol and humidity to the nostril inlets.

solution with a nebulizer gas flow rate of 7 L/min and a drying gas flow rate of 3 L/min. Previous analysis indicated that the droplets of the 900 nm aerosol produced by the SPAG retained an aqueous component and contained 49% albuterol sulfate by mass.[34] Aerosols were generated and delivered into the nasal airway model for 30 sec, which was sufficient to produce quantifiable drug deposition in both the nasal geometry and the cascade impactor.

For the control experiment, a commercially available hand-held nebulizer was employed to deliver a standard medical aerosol to the nasal model. A Fisoneb ultrasonic nebulizer (Fisons Corp., Rochester, NY) was used to generate an aerosol with a 4.67-μm mass median aerodynamic diameter (MMAD) using a 0.5% albuterol sulfate in water solution for 20 sec, which was sufficient to produce quantifiable drug deposition in both the nasal geometry and the cascade impactor. The GSD of the initial Fisoneb aerosol was 1.73.

Experimental drug deposition and aerosol size assessment

Following each aerosol generation experiment, the NMT model was disassembled and wall washings were taken. Appropriate volumes of water (25–50 mL depending on the expected final albuterol concentration) were used to collect albuterol sulfate deposited on the walls of the model. The mean (SD) amount of drug deposited in the NMT was determined by quantitative HPLC albuterol sulfate analysis of washing obtained from the model surfaces. The NMT deposition fraction was reported as a percentage of the total delivered dose of albuterol sulfate. The particle size distribution and mass of drug delivered to the impactor were also determined following aerosol generation. Washings were collected from the impaction plates to determine the drug deposition using appropriate volumes of water. The solutions were then

assayed using the quantitative HPLC method. The mass of drug on each impaction plate was determined and used to calculate the final aerodynamic particle size distributions of the drug aerosols. Aerosol droplet size distributions were reported as albuterol sulfate mass distribution recovered from the impactor. The mass median aerodynamic diameter (MMAD) was defined as the particle size at the 50th percentile on a cumulative percent mass undersize distribution (D50) using linear interpolation. The mean (SD) total delivered dose was determined as the sum of the drug recovered from the nasal model and the cascade impactor.

CFD simulations

A CFD model was implemented that can accurately simulate local temperature and humidity fields, together with droplet trajectories, size change, and deposition within the NMT model during the ECG process. Considering the flow field, laminar, transitional, and turbulent conditions are expected. To effectively address this broad range of flow conditions, a low Reynolds number (LRN) k$-\omega$ turbulence model was selected. This model has previously been well tested, and found to provide good estimates of aerosol transport and deposition in upper airway models.[52–54] To evaluate the variable temperature and RH fields in the NMT model, interconnected relations governing the transport of heat and mass (water vapor) were also included. These governing equations were previously presented in detail by Longest and Xi[37] and Longest et al.[55]

To model droplet trajectories, growth, and deposition, a previously developed and tested combination of a commercial code (Fluent 6.3, ANSYS Inc., Cannonsburg, PA) and user functions was implemented. User routines were employed to better model near-wall conditions and to simulate aerosol condensation and evaporation in the complex three-dimensional temperature and humidity fields. Previous studies have shown that the isotropic turbulence approximation, which is assumed with the LRN k$-\omega$ model, can overpredict aerosol deposition.[56] As a result, a user routine was employed to account for anisotropic near-wall turbulence, as described by Longest et al.[55] Other additions to the particle tracking model included (1) a correction to better predict the Brownian motion of submicrometer aerosols and (2) improved near-wall interpolation of fluid velocities.[57]

A user routine was employed to model interconnected droplet temperature and size change resulting from condensation and evaporation. This droplet model accounts for the Kelvin effect, hygroscopicity arising from the dissolved drug, and the effect of droplet temperature on surface vapor pressure. Experimental measurements were made to accurately predict activity coefficients for albuterol sulfate dissolved in water through a range of concentrations. A rapid mixing model approach was employed to simulate droplet heat and mass transfer, which assumes spatially constant temperature and concentration values within each droplet. Application of the RMM approach to inhaled respiratory aerosols was previously validated by Longest and Kleinstreuer.[58] The droplet heat and mass transfer relations are described in detail by Longest and Hindle.[32] In simulating aerosol evaporation and growth, the effect of the droplets on the continuous phase was typically neglected, resulting in a one-way coupled approach. To assess the validity of this assumption, the effect of the discrete aerosol phase on the continuous heat and water vapor fields was also included in some simulations, which is referred to as two-way coupling. An experimentally measured concentration of 2.8×10^5 particles/cm^3 for the 900-nm aerosol (after mixing with the humidity stream) was employed to assess the two-way coupling effects. Aerosol concentration was measured (CPC 3022A, TSI Inc, Shoreview, MN) after mixing with the humidity stream and sampled at 25 cm^3/sec following passage through a condensational growth tube, as reported by Longest and Hindle.[34]

The CFD model employed in this study has previously been tested in comparison with experimental deposition results. For both constant-sized particles and evaporating droplets, the CFD model was shown to accurately predict local and sectional deposition profiles in comparison with *in vitro* experiments.[53,59,60] Good agreement with experimental deposition results has been shown for both nano- and micrometer aerosols.[52,57] Longest and Hindle[32] recently presented a CFD model of ECG aerosol delivery in detail. In this study, excellent agreement was found between experimental measurements of final particle size after condensational growth and CFD predictions. Hindle and Longest[35] compared *in vitro* results and numerical predictions of aerosol drug deposition in a MT and TB geometry extending to the fifth respiratory generation. Good agreement was found between the experimental and numerical predictions of deposition for both control and ECG conditions on a sectional basis and for the entire MT–TB geometry.

In performing the CFD simulations, previously established best practices were implemented to provide a high quality solution. All transport equations were discretized to be at least second order accurate in space and time. The computational mesh was constructed in Gambit 2.4 (ANSYS, Inc.) and consisted entirely of tetrahedral grid elements surrounded by a near-wall layer of high-resolution pentahedral cells. Previous studies by Xi and Longest[41,42] and Xi et al.[54] have demonstrated that this grid configuration can provide a good match to experimental aerosol deposition data in the upper respiratory airways. Convergence of the flow field solution was assumed when the global mass residual had been reduced from its original value by five orders of magnitude and when the residual reduction rates for both mass and momentum were sufficiently small. To improve accuracy and to better resolve the significant change in flow scales during deposition, all calculations were performed in double precision. For the NMT model, grid convergent results were found to occur with meshes consisting of approximately 2.4 million control volumes. In order to produce convergent deposition results for all droplet sizes considered, groups of 3000 droplets were released to represent each of the 9 size bins considered, resulting in 27,000 tracked elements. The final mass deposition results were scaled to reflect the experimentally determined initial aerosol size distribution for comparison with the measured deposition fractions of drug mass and final MMAD. Doubling the number of droplets considered had a negligible impact on both total and sectional deposition results.

Delivery conditions

Both *in vitro* experiments and CFD simulations were used to compare standard nebulizer aerosol delivery (Case

Table 1. Airflow, Aerosol, and Wall Conditions of the Four Cases Considered

Cases	*Aerosol inlet (right nostril)*	*Humidity inlet (left nostril)*	*Wall conditions*
1 (EXP/CFD)	Q: 10 L/min T: 37°C *RH*: 99% MMAD = 4.67 (0.05) μm $n = 3.0\times10^5$ part/cm^3	Q: 20 L/min T: 25°C *RH*: 100%	T_{wall} : 37°C RH_{wall} : 0%[a]
2 (EXP/CFD)	Q: 10 L/min T: 21°C *RH*: 97.5% MMAD = 900 (32.7) nm $n = 2.8\times10^5$ part/cm^3	Q: 20 L/min T: 39°C *RH*: 100%	T_{wall} : 37°C RH_{wall} : 100%
3 (CFD)[b]	Q: 15 L/min T: 35°C *RH*: 95% MMAD = 560 (11.4) nm and 900 (32.7) nm	Q: 15 L/min T: 39°C *RH*: 100%	T_{wall} : 37°C RH_{wall} : 100%
4 (CFD)[b]	Q: 15 L/min T: 35°C *RH*: 95% MMAD = 560 (11.4) nm and 900 (32.7) nm	Q: 15 L/min T: 42°C *RH*: 100%	T_{wall} : 37°C RH_{wall} : 100%

[a]Humidified air was insufficient to wet the airway walls in the experiment for Case 1. Dry walls were included in the CFD simulation to match the *in vitro* conditions.
[b]CFD simulations were used to explore the effects of modifying the aerosol and humidity inlet conditions.

1—control) and the ECG approach (Case 2). Flow field and aerosol conditions for these cases are based on experimental measurements made at the NMT model inlets and are reported in Table 1. For all cases considered, the aerosol stream was delivered to the right nostril and humidity was delivered to the left nostril. The mouth opening of the model was sealed so that there was no inlet or outlet flow. Steady flow conditions were considered with a combined flow rate of approximately 30 L/min passing through the geometry. Considering the control case, the Fisoneb ultrasonic nebulizer produced an aerosol with a MMAD (standard deviation) of 4.67 (0.05) μm and a concentration of 3×10^5 particles/cm^3 entering the NMT model. To avoid evaporation and drying of the nebulized aerosol, it was transported to the nasal inlet using heated and humidified co-flow air ($T = 37$°C and 99% RH) at a flow rate of 10 L/min. Humidified but unheated air was delivered to the other nostril for the control case. The experimental ECG conditions (Case 2) consisted of the 900 nm aerosol delivered to the right nostril at a flow rate of 10 L/min under subsaturated conditions ($T = 21$°C and 97.5% RH). The humidified airstream was delivered to the left nostril at saturated conditions (100% RH) and a temperature of 39°C.

In addition to Cases 1 and 2, CFD simulations were also used to investigate the effects of the initial aerosol size (MMAD = 560 nm and 900 nm) and increasing the delivery temperatures (Table 1). For Case 3, ECG conditions were employed for both 560 and 900 nm particles with aerosol and humidity airstream temperatures of 35 and 39°C, respectively. Case 4 was identical to Case 3, but with the temperature of the saturated airstream increased to 42°C, which delivers significantly more water vapor mass to the airways. For Cases 3 and 4, the flow rate of the aerosol and humidity streams were also matched at 15 L/min each.

Wall temperatures were maintained at 37°C in all cases, to approximate *in vivo* conditions. For the ECG cases, the airway walls in the experiments were preconditioned with supersaturated air to produce an initially wet surface. Wet airway walls were also assumed in the ECG simulations, which were implemented as a saturated mass fraction of water vapor at the boundary ($RH_{wall} = 100\%$). However, the airway walls of the control case were not prewetted in the experiments and simulations. Walls of Case 1 were dry to foster aerosol evaporation and thereby minimize deposition, resulting in the best possible performance of the control. For the numerical simulation of Case 1, the walls were assumed dry to best approximate the experimental conditions. In the experiments, aerosol deposition can wet the walls leading to subsequent evaporation; however, this level of complexity was not included in the model. An additional case was also considered to evaluate the effects of variations in nasal wall temperature.

Results

Continuous field variables

Mid-plane and cross-sectional contours of temperature profiles based on CFD predictions are shown in Figure 2 for the four inlet cases considered. For all inlet conditions, the narrow nasal passages are observed to quickly equilibrate the air temperature to wall conditions (i.e., 37°C). As a result, temperatures in the pharyngeal and laryngeal portions of the geometry only vary from wall boundary conditions by a maximum of several degrees. Case 1 is observed to have the lowest MT temperatures, which range from 34–37°C, and are due to the humidified airstream entering the model at 20 L/min and 25°C (Table 1). Introducing warm saturated airflow in Case 2 raises the MT temperatures to the range of 36–38°C.

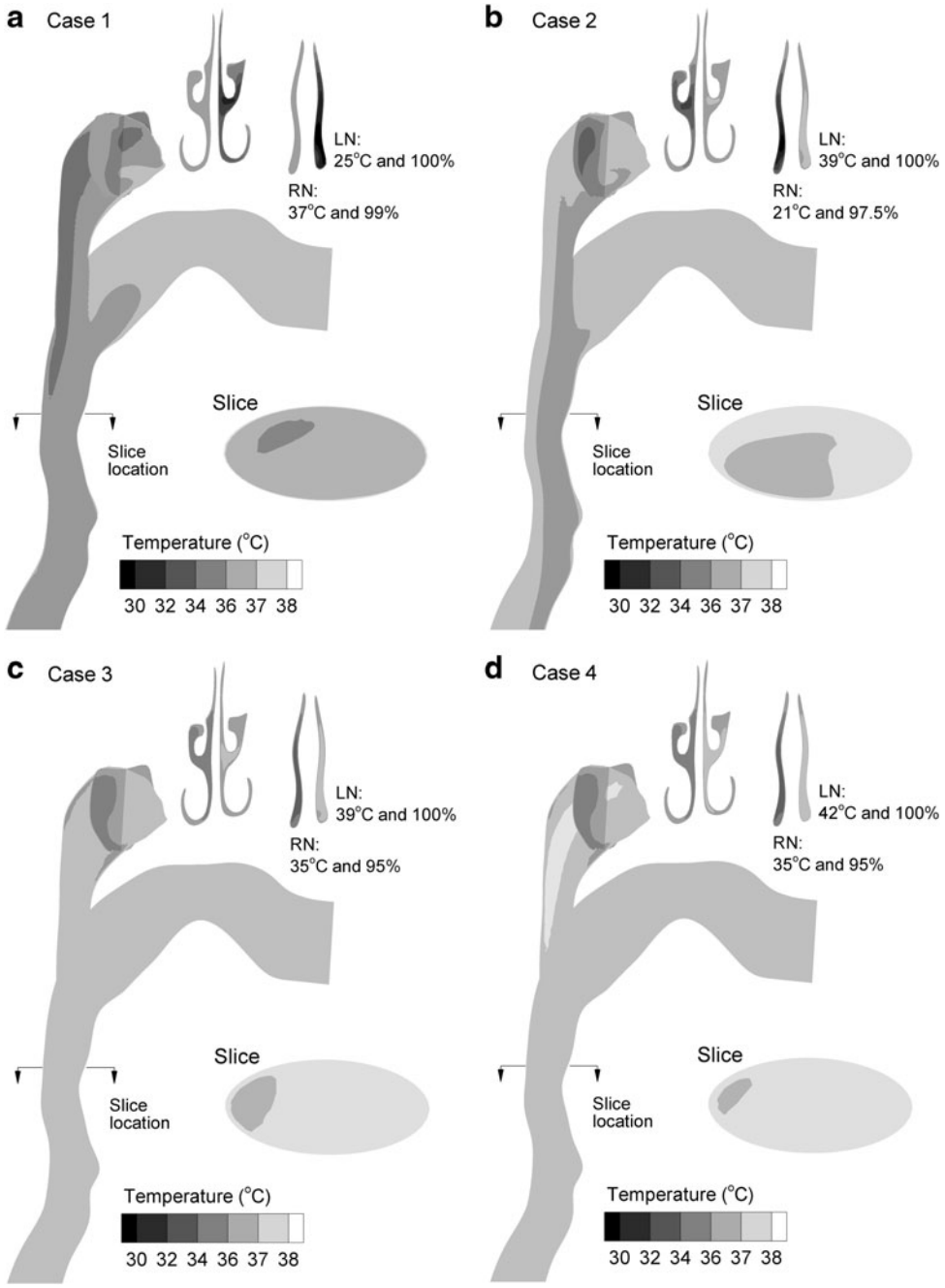

FIG. 2. Contours of temperature at the midplane and selected cross-sectional locations for the inlet conditions of (**a**) Case 1, (**b**) Case 2, (**c**) Case 3, and (**d**) Case 4. The inlet and wall conditions for each case are described in Table 1. Left and right nostril conditions are abbreviated in the figure as LN and RN, respectively.

Finally, heating both the aerosol and humidity streams (Cases 3 and 4) results in MT temperatures in the range of 37–38°C, with a region greater than 38°C observed in the nasopharyngeal section of Case 4.

Predicted contours of RH are displayed for midplane and cross-sectional slices in Figure 3 based on CFD simulations. Considering the control scenario (Case 1), heating of the initially cool humidified airstream and dry walls produce subsaturated conditions. Relative humidity values in the MT region are less than 10%, which is expected to result in significant aerosol evaporation for Case 1. In contrast, cooling of the humidified airstream under ECG conditions is observed to produce supersaturation with RH values above 100%. As with temperature, the nasal passages quickly equilibrate the air phase relative humidity to near wall boundary conditions (i.e., $RH_{wall} = 100\%$). However, zones of supersaturation are observed in the MT region with all ECG cases. Surprisingly, higher RH values are observed in the MT region of Case 2 compared to Case 3. This is likely because mixing of the initially 21°C aerosol stream and 39°C humidified air in the nasopharynx produces higher supersaturation values for Case 2, which progress downstream. For both Case 2 and Case 3, supersaturated RH values remain in the range of 100–101%. Only for a humidified inlet temperature of 42°C

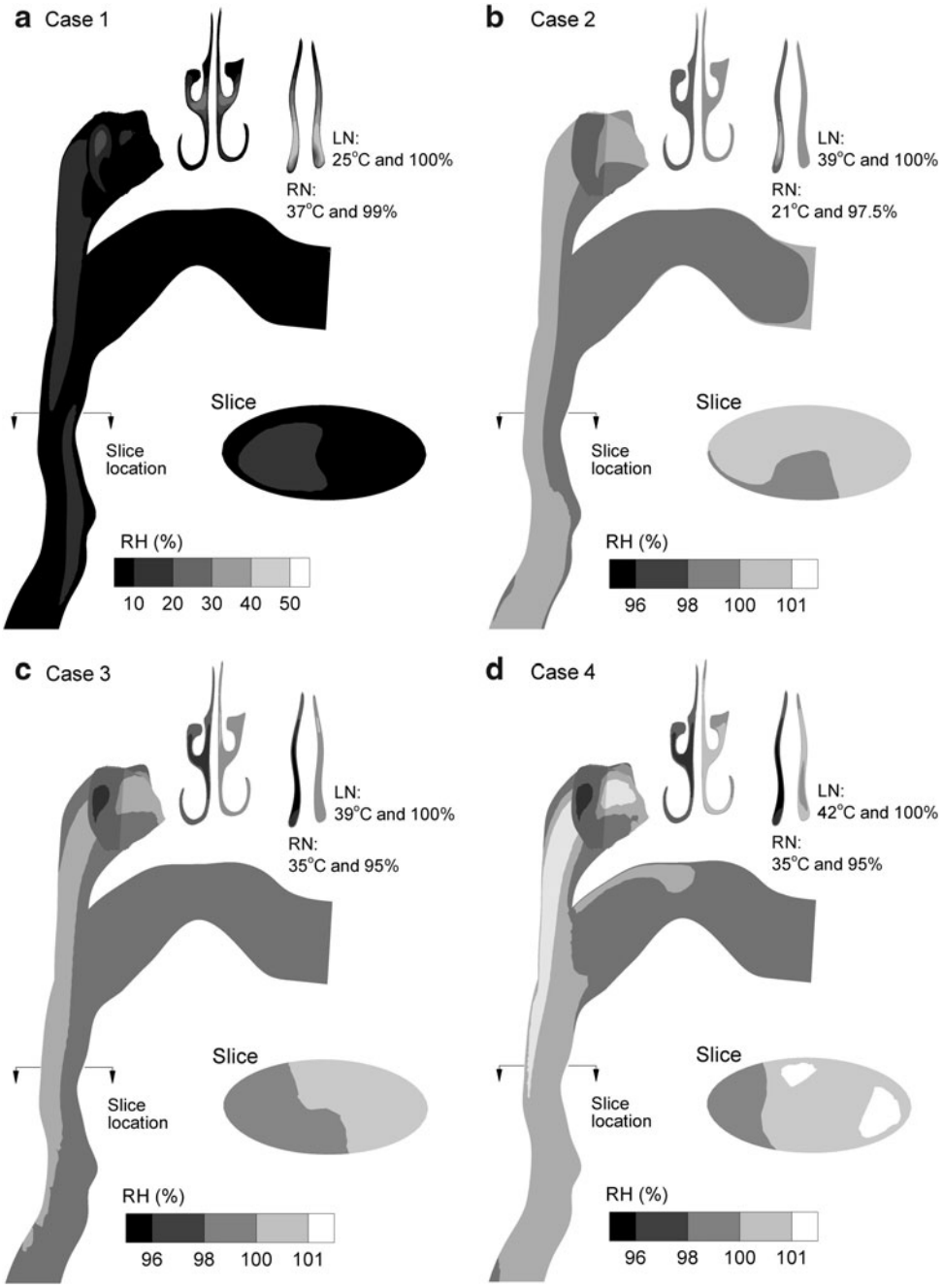

FIG. 3. Contours of relative humidity at the midplane and selected cross-sectional locations for the inlet conditions of (**a**) Case 1, (**b**) Case 2, (**c**) Case 3, and (**d**) Case 4. The inlet and wall conditions for each case are described in Table 1. Supersaturated conditions are observed in the nasopharyngeal and more distal regions of Cases 2–4.

(Case 4) are RH values greater than 101% observed. Although these supersaturation levels may appear low, Longest and Xi [37] and Longest et al.[34] demonstrated that fractional increases in RH above 100% can dramatically increase the rate of condensational growth for an aerosol in the size range of 1 μm.

Trajectories and size increase

To illustrate droplet size change in the calculated RH environments, trajectories of droplets contoured according to size are displayed in Figure 4 for each of the four cases considered. To illustrate trajectories, approximately 200 monodisperse droplets were seeded with a diameter equal to the measured MMAD in each case (4.67 μm—control vs. 900 nm—ECG). As expected with Case 1, the low RH conditions produce significant evaporation until only dried drug particles with a diameter of approximately 0.8 μm remain. In contrast, appreciable droplet size increase is observed for each of the ECG conditions. With Case 2, growth begins within the nasal cavity airway as a result of airstream heating and concurrent mass transfer. This growth continues in the nasopharynx and MT regions as the supersaturated humidity and aerosol streams mix. For Cases 3 and 4, growth is

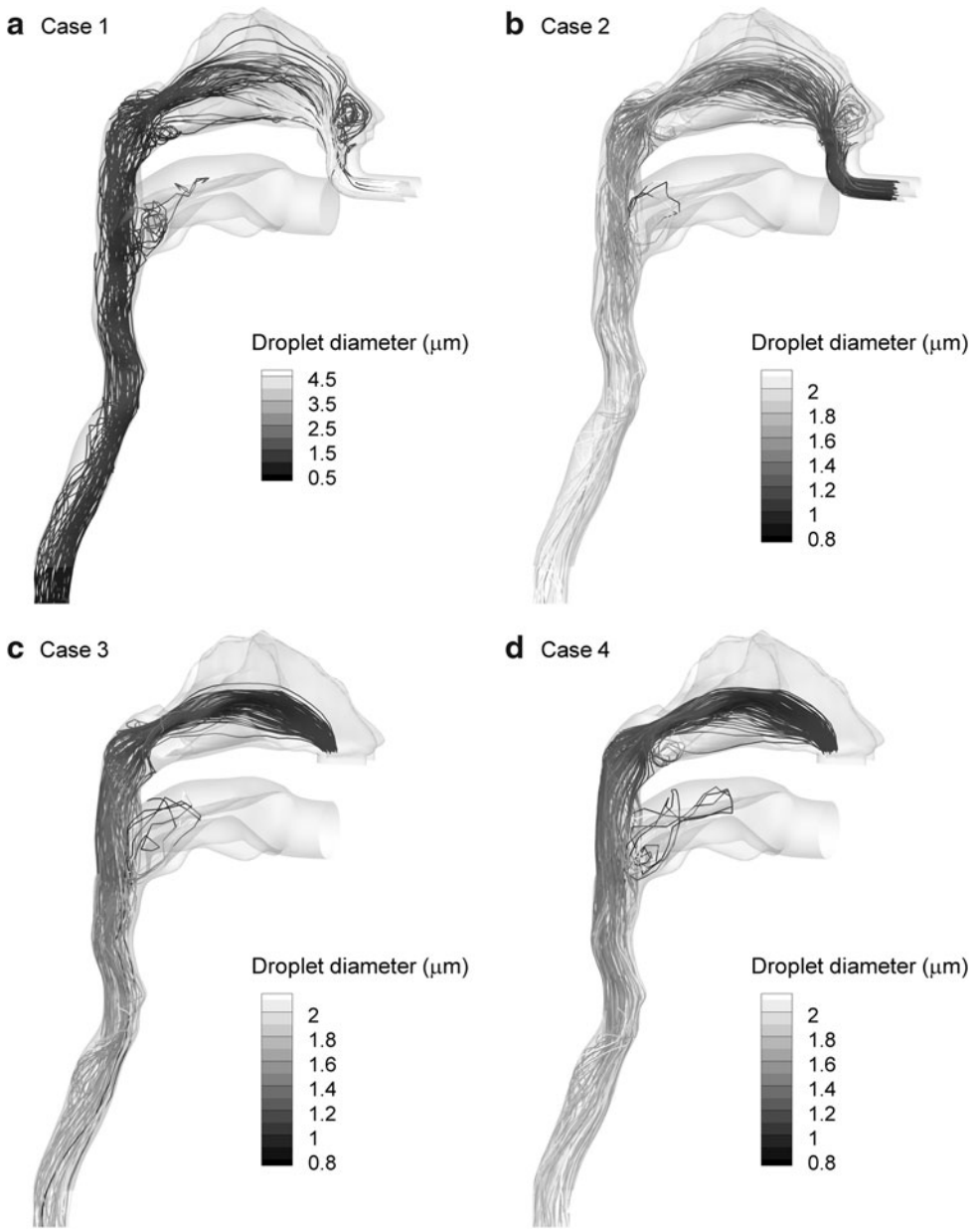

FIG. 4. Representative trajectories of initially monodisperse droplets for the inlet conditions of (**a**) Case 1, (**b**) Case 2, (**c**) Case 3, and (**d**) Case 4. Initial droplet sizes were 4.67 μm for Case 1 and 900 nm for the remaining ECG cases. Significant evaporation is observed for Case 1 due to dry model walls and subsaturated airfield conditions. In contrast, significant aerosol growth is observed for the remaining cases where cooling of the airstream and wet airway walls produce supersaturated conditions.

distinctively absent in the nasal passages due to the increased aerosol temperature. Growth then begins in the nasopharynx region and continues downstream. Some additional growth is visible from the trajectory contours with Case 4 compared to Case 3. Furthermore, it is observed that a very small fraction of the aerosol enters the oral cavity, even for the relatively wide mouth opening included in the NMT model.

Experimental and numerical predictions of outlet MMAD aerosol sizes and GSD are provided in Table 2 for Cases 1 and 2. The numerical predictions of MMAD are based on simulations that employed the experimentally measured initial size distributions as the starting aerosol conditions. Additional CFD estimates of aerosol size are also provided at the sectional division between the nasal and MT regions, shown in Figure 1. For Case 1 conditions, good agreement is observed between the experimental measurements and numerical predictions [0.8 (SD = 0.3) μm vs. 0.73 μm]. This finding confirms that significant evaporation occurs under Case 1 conditions, which include warm dry walls. Considering Case 2, the experimentally measured outlet MMAD (SD) was 1.88 (0.09) μm compared with a CFD prediction of 2.29 μm. The difference between these two values results in a relative error of 20%, which is acceptable considering

Table 2. Comparison of Experimental and CFD-Predicted Aerosol Size for Cases 1 and 2

	Size at sectional division[a]		*Size at model outlet*	
Case 1	MMAD μm	GSD	MMAD (SD) μm	GSD
Experiment 4.67[b] μm aerosol	NA	NA	0.8 (0.3)[c]	2.49
CFD 4.67 μm aerosol	0.74	2.26	0.73[d]	2.27
Case 2				
Experiment 900 nm aerosol	NA	NA	1.88 (0.09)	1.65
CFD 900 nm aerosol (one-way coupling)	1.91	1.53	2.29	1.35
CFD 900 nm aerosol (two-way coupling)	1.85[e]	1.55	2.25[e]	1.37

[a]Division between the nasal and pharyngeal sections of the model (see Fig. 1).
[b]Initial MMAD of the aerosol at the model inlet.
[c]Values representing experimental standard deviations (SD) are reported in parentheses.
[d]CFD predictions within ± 1 SD of the experimental value.
[e]The inclusion of two-way coupling did not significantly affect the final MMAD.

the complexity of the system. In this study, relative percent errors of, for example, MMAD are calculated as $(|MMAD_{CFD} - MMAD_{Exp.}|/MMAD_{Exp.}) \times 100$.

As described, the computational predictions in this study are based on a one-way coupled assumption, which neglects the effects of the discrete phase on the continuous field. As shown by Longest et al.,[34] this assumption may be responsible for overpredicting the aerosol growth rate and final aerosol size. However, two-way coupled simulations of Case 2 produced a final aerosol size of 2.25 μm, which is approximately equal to the one-way coupled result (Table 2). Therefore, the effects of two-way coupling do not appear to be significant in the current system, potentially due to the presence of wetted airway walls and the amount of water mass supplied by the humidity stream.

Predictions of MMAD and GSD for Cases 3 and 4 are presented in Table 3 based on CFD calculations. In addition to the 900 nm aerosol, an aerosol with an initial MMAD of 560 nm was also considered, which was generated and reported in the experimental study of Longest et al.[34] For Cases 3 and 4, the initial size difference between the two aerosols of approximately 340 nm is maintained at the sectional division and model outlet as growth occurs (Table 3). Little difference in the aerosol MMAD is observed between the two cases at the nasal outlet, for each initial size. However, the MMADs at the NMT model outlet for Case 4 are approximately 300 nm greater than with Case 3. Both Cases 3 and 4 with an initial 900 nm aerosol produce an outlet MMAD near 2 μm or greater.

Table 3. CFD Predictions of Aerosol Size for Cases 3 and 4

	Size at sectional division[a]		*Size at model outlet*	
Case 3	MMAD μm	GSD	MMAD μm	GSD
CFD 560[b] nm aerosol	1.04	1.74	1.42	1.39
CFD 900 nm aerosol	1.44	1.35	1.89	1.52
Case 4				
CFD 560 nm aerosol	1.09	1.65	1.70	1.45
CFD 900 nm aerosol	1.50	1.34	2.10	1.45

[a]Division between the nasal and pharyngeal sections of the model (see Fig. 1).
[b]Initial MMAD of the aerosol at the model inlet.

Further details of the predicted aerosol growth for Cases 3 and 4 are presented in Figure 5 as size distributions. It is observed that a portion of the exiting aerosol size distribution is in the submicrometer range in some cases. This submicrometer fraction may be due to the Kelvin effect, which slows the condensational growth of the smallest nanoparticles in the system. For Case 3, the submicrometer fraction decreases between the sectional division and model outlet, but remains present. It is not clear if this submicrometer fraction will be eliminated with further growth downstream. Under Case 4 conditions, a submicrometer fraction is observed at the sectional division, but is eliminated at the model outlet.

Deposition

Deposition fractions in terms of drug mass based on CFD predictions and experimental results are presented in Figure 6 for Cases 1 and 2. The division between the nasal and MT regions is shown in Figure 1. With Case 1 conditions, the CFD model predicts approximately 59.2% drug deposition in the nasal cavity and 6.5% in the MT region. The total predicted deposited dose of 65.7% is in relatively good agreement with the experimental value (SD) of 72.6 (3.7) %. For ECG conditions (Case 2), the predicted nasal deposition fraction is reduced to 13.4% with 2.5% deposition in the MT. The total predicted deposited dose of 15.9% provides an excellent estimate of the *in vitro* value of 14.8 (1.83)%. As a result, it is concluded that ECG conditions largely reduce the total extrathoracic deposition compared with the control case and that the CFD model accurately predicts the total deposited drug mass.

Predictions of aerosol deposition on a local basis for Cases 3 and 4 are provided in Figure 7. For both cases, significantly less aerosol deposition is observed in the nasal cavity compared with Case 2, and is between 1 and 2%. This reduction is likely because of the delayed aerosol growth observed with Cases 3 and 4 (Fig. 4), even though the flow rate of the aerosol stream is increased to 15 L/min. Aerosol deposition in the MT region increases by approximately 1% for Cases 3 and 4 compared with Case 2, which is a negligible change. As a result, the total deposition fraction for these ECG cases

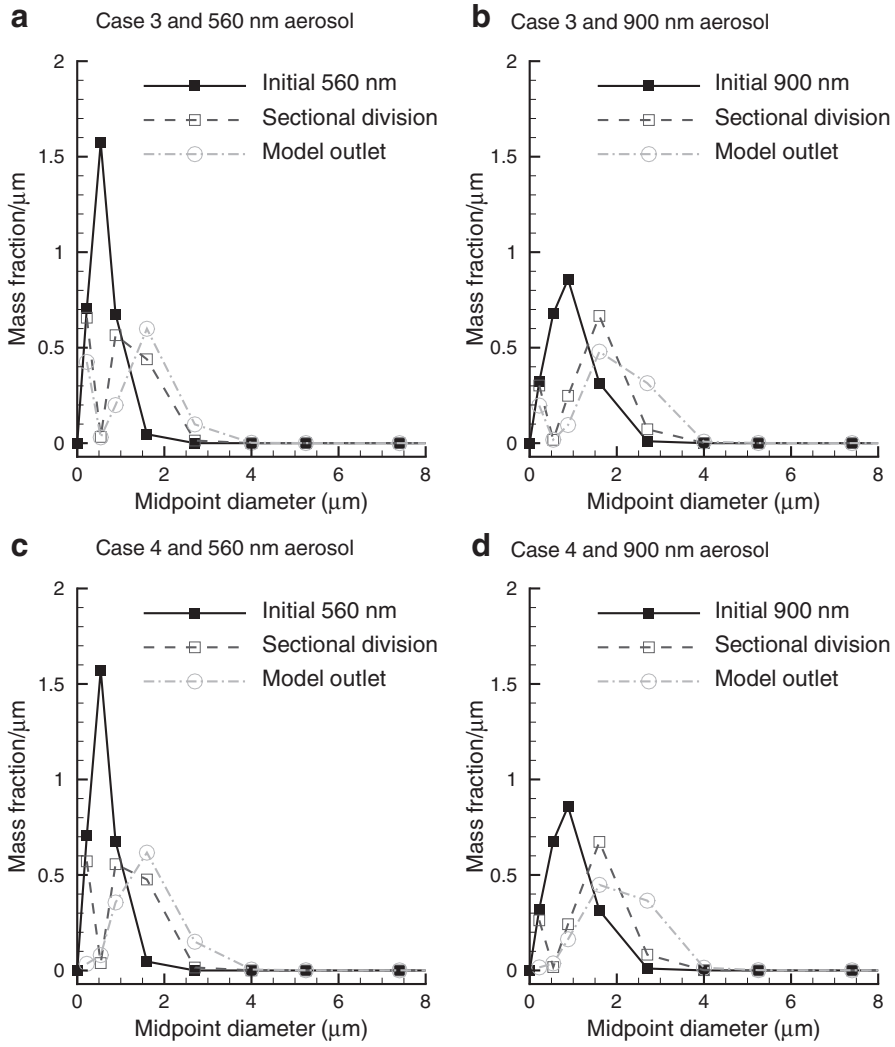

FIG. 5. Aerosol size distributions in terms of mass fraction per micrometer at the nasal inlet, sectional division (Fig. 1) and model outlet for Case 3 conditions with (**a**) 560 nm and (**b**) 900 nm aerosols; and for Case 4 conditions with (**c**) 560 nm and (**d**) 900 nm aerosols.

is approximately 5%, which provides a significant reduction in deposition compared to Case 2 conditions. From Figure 7 it is observed that a majority of the deposited droplets are approximately 1–3 μm, which likely contact the wall due to turbulent dispersion and impaction. Droplets in the size range of 2–3 μm are observed on the wall near the outlet for Case 3 and at a higher frequency for Case 4.

Effects of nasal wall temperature

It is expected that the airway wall temperature will be below 37°C in a portion of the nasal cavity and then increase to core body temperature at some point along the flow passages. To investigate the effects of variable wall temperature on ECG delivery, an additional case was considered in which the temperature of the nasal airways was 35°C, and the wall temperature was increased to 37°C at the sectional division inlet to the MT. Delivery conditions were otherwise equal to those of Case 3, as shown in Table 1. Due to the reduced wall temperature, RH values are highest in the nasopharyngeal region (Fig. 8b) compared with the previous three results. However, the outlet MMAD of 1.8 μm is essentially unchanged from the constant wall temperature condition. Figure 8b also illustrates continued aerosol growth beyond the NMT geometry outlet. At the approximate location of the first bifurcation, the median aerosol size is now approximately 2 μm. Finally, the variable wall temperature case results in a total drug deposition fraction in the NMT model of 5.6%, which is not appreciably changed from the constant wall temperature case.

Discussion

In this study, ECG was explored as a method to improve aerosol delivery through the complex nasal passages and MT geometry during NIV. *In vitro* experiments showed that the ECG approach could significantly reduce the drug deposition fraction in the NMT geometry compared with the control case [14.8 (1.83)%—ECG vs. 72.6 (3.7)%—control]. Aerosol size was also shown to increase from an initial MMAD of 900 nm to a target size of approximately 2 μm at the exit of the NMT geometry. Results of the CFD model

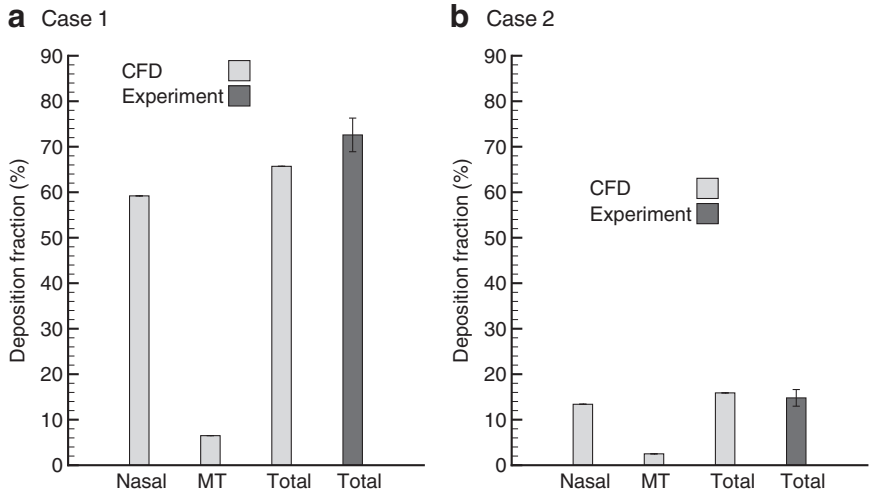

FIG. 6. Comparison of deposition fractions between the CFD model predictions and experimental results expressed as a percentage of total drug mass delivered. Nasal includes the nasal cavity and nasopharyngeal regions, whereas MT contains the remainder of the geometry (pharynx, mouth, larynx, and upper trachea). The sectional division is marked in Figure 1. Model results are in close agreement with experimental predictions of total deposited drug mass.

were in good agreement with the experimental findings, which provided confidence that the model was sufficiently accurate for the simulation of ECG aerosol delivery. Specifically, CFD predictions of aerosol growth were within a 20% relative error of the experimental findings and predictions of ECG deposition fractions produced relative errors as low as approximately 5%. The CFD model was then used to explore the effects of additional delivery conditions. By increasing the delivery temperature of the aerosol stream from 21 to 35°C, total deposition in the NMT geometry was reduced to approximately 5% and outlet aerosol size remained at approximately 2 μm or greater, based on CFD predictions. Differences in initial aerosol size (560 vs. 900 nm) were maintained through the model during aerosol growth, which in comparison to the results of Longest et al.[34] indicates that size increase is not complete at the model outlet. Reducing the airway wall temperature of the nasal passage from 37 to 35°C did not appreciably affect the outlet aerosol size or the

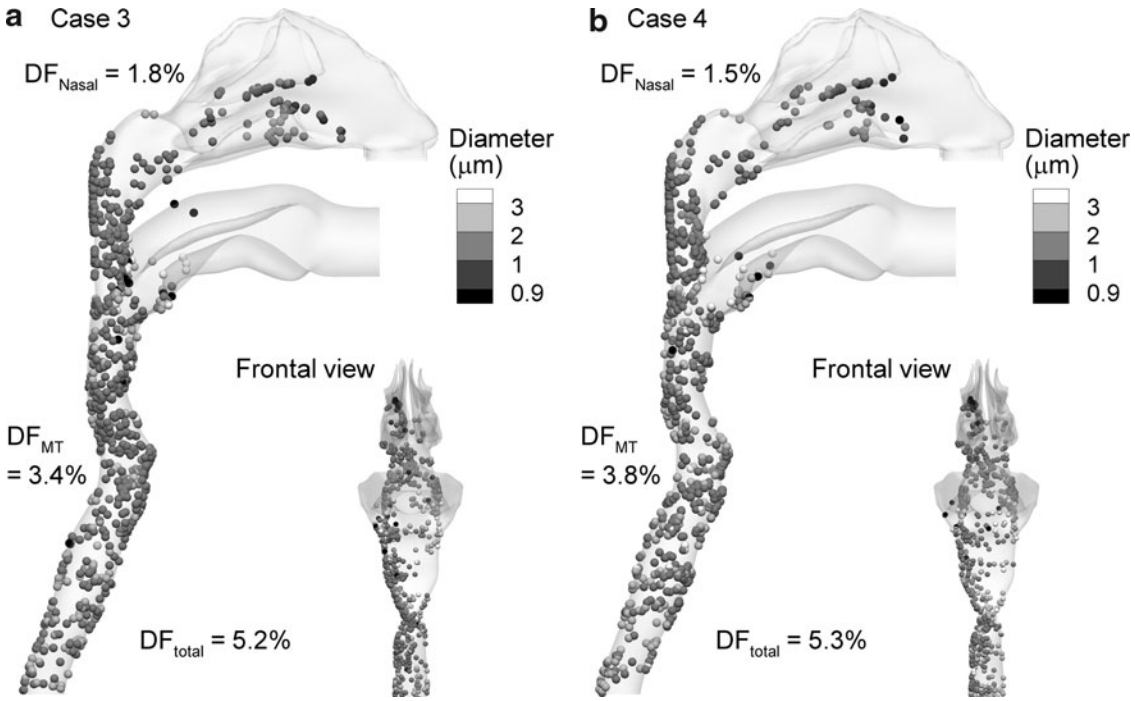

FIG. 7. Deposition locations and final aerosol diameters of initially 900 nm monodisperse droplets for (**a**) Case 3 and (**b**) Case 4 inlet conditions. Very little deposition is observed in the nasal cavity. The reported deposition fractions (DF) are expressed as percentages of the delivered dose and are based on the experimental aerosol size distribution.

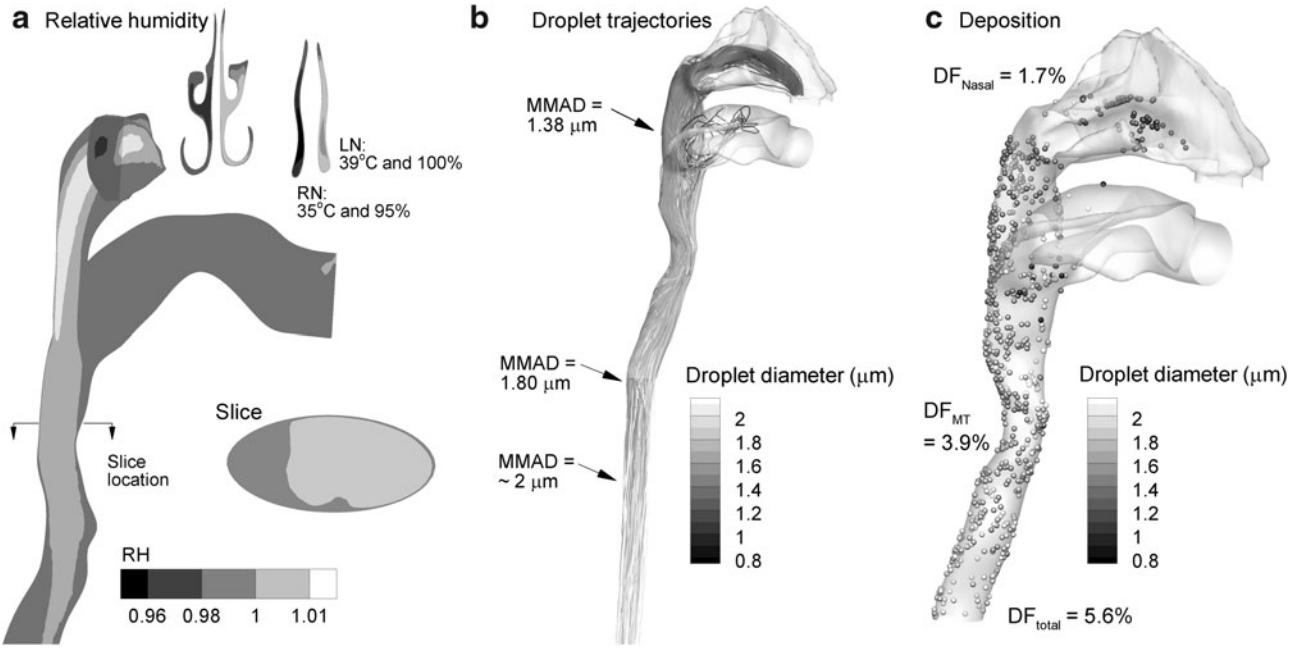

FIG. 8. Characterization of aerosol growth for a nasal temperature of 35°C and a temperature of 37°C in the remainder of the geometry under Case 3 conditions in terms of (**a**) relative humidity, (**b**) trajectories of initially monodisperse 900 nm droplets, and (**c**) deposition locations of 900 nm droplets.

total deposition fraction, which remained around 2 μm and 5%, respectively.

This study demonstrates that ECG may substantially improve pharmaceutical aerosol delivery through the complex nasal and extrathoracic airways. Expected high deposition in the nasal passages has previously been a barrier to the effective delivery of aerosols through the nose and into the lungs. However, depositional losses were not assessed in the delivery system as with the study of Bhashyam et al.,[16] and a typical patient interface used with NIV systems was not included. Moreover, flow conditions consistent with HFT ventilation were employed. Although depositional losses in the aerosol generation and delivery lines were not assessed, it is expected that the use of submicrometer aerosols will greatly reduce inertial deposition, gravitational settling, and turbulent dispersion.[40,61,62] As a result, depositional losses in the aerosol generation and delivery systems will be greatly reduced. Submicrometer aerosols are also expected to largely eliminate deposition in the NIV patient interface, which may be a nasal cannula or face mask. Therefore, the ECG approach may significantly improve aerosol depositional losses associated with delivery using HFT and NPPV systems. Considering application of ECG during NPPV, temperatures and RH may need to be increased to match the values considered in this study in order to foster sufficient size growth for pulmonary deposition. The total flow rate of 30 L/min is typical for adult HFT,[2] but will need to be reconsidered for low-flow therapy and NPPV systems. Hygroscopic excipients may potentially be included if the growth of the aerosol is insufficient to foster full lung deposition.[63] Delivery of the aerosol to the more patent nostril of an individual should also be considered. Additional studies are needed to better assess deposition in the delivery system and patient interface, as well as to tailor the condensational growth approach to individual NIV systems. However, the results of the current study coupled with these observations suggest that the ECG approach may be a practical method to deliver aerosols to the lung during NIV with the potential for less than 10% depositional loss and 90% or greater pulmonary retention.

One initially unexpected finding of the current study was that condensational growth occurred in the right nasal passage under Case 2 delivery conditions, before mixing with the supersaturated airstream. In Case 2, the aerosol was delivered at 21°C with 97.5% RH. Typically, supersaturation is expected to occur during the cooling of saturated or near-saturated air. However, results of this study show that supersaturation can also occur for a cool humid airstream passing through a channel with warm wet walls. This phenomena was previously observed in aerosol growth studies and is the working principle behind many current water-based condensation particle counters.[64] Moreover, previous computational studies by Ferron et al.[65] and Zhang et al.[66] have observed mild supersaturation in the upper airways during the inhalation of cool saturated air. The results of this study indicate that increasing the inhaled temperature of the aerosol to near airway wall conditions (Cases 3 and 4) can reduce aerosol growth in the nasal passages prior to mixing with the supersaturated airstream. This provides one explanation of why aerosol deposition in the nasal passages was reduced for Cases 3 and 4 (1–2%) compared with the Case 2 CFD result (~13%). Therefore, it is recommended that the aerosol stream be near body temperature conditions to maximize the effectiveness of ECG delivery.

In this study, good agreements were found between the experimental results and numerical predictions; however, some differences were observed. Considering total deposition fractions of drug in Case 1, the relative error between the experimental and numerical values [72.6 (3.7)%—experiment

vs. 65.7%—CFD] was 9.5%. This difference may arise from wall roughness effects in the *in vitro* model, which increase the deposition of larger aerosols as reported by Kelly et al.[29] and Shi et al.[67] For Case 2 conditions, which started with a smaller aerosol size of 900 nm, the numerical predictions of drug deposition fraction were within the SD range of the experimental result.

Considering predictions of final aerosols size, the numerical values were generally higher than the experimental results with a maximum relative error of 20%. Based on the previous results of Longest and Hindle,[32] it was expected that aerosol growth had reduced the amount of water vapor in the air and limited the final size increase, that is, two-way coupling. However, including two-way coupling effects in the simulation had a negligible impact on final aerosol size in this study. This is likely because the combination of prewetted walls and supersaturated airflow provide sufficient water mass for unrestricted growth within the NMT geometry. Instead, differences in the experimental and numerical results may be primarily due to experimental difficulties associated with assessing final aerosol size. Some size increase may occur in the impactor, which is expected based on the observation that growth is continuing at the model outlet. However, assessing flow conditions in the complex impactor geometry, as shown by Vinchurkar et al.,[68] was beyond the scope of this study. Furthermore, the airway walls were prewetted in the experimental ECG case. Drying of this initially wet boundary condition over the course of the experiment may have limited the final aerosol size compared to the CFD simulations. Considering these complexities, agreements between the CFD model and experimental results appear quite good.

In addition to the limitations described above, other assumptions include the use of a single idealized NMT geometry, steady flow conditions, and a two-equation turbulence model. The NMT geometry used in this study is intended as an idealized representation of adult airways, which is a combination of representative MT and nasal models. Theoretically, reduced extrathoracic deposition associated with ECG delivery should largely decrease variability in deposition associated with the geometry.[31] However, further studies are needed in patient specific extrathoracic models developed from individuals to assess the effects of the current approximate model, intersubject variability, and to extend the ECG delivery approach to children and infants. Furthermore, the airflow through commercially available nasal cannula may introduce flow field artifacts that are different from the simple models considered in this study. Current cannula designs will likely need to be modified to allow for efficient delivery of even submicrometer aerosols. In this study, only steady flow conditions were considered. For effective aerosol delivery, intermittent aerosol generation during inspiratory flow will be necessary, which is currently employed with administration during invasive mechanical ventilation. Transient inspiration is expected to more significantly influence the deposition of larger aerosols compared with submicrometer droplets, as delivered with ECG.

In conclusion, an ECG delivery approach was shown to significantly reduce aerosol depositional losses in a NMT geometry compared to a control case and produce an aerosol of approximately 2 μm or greater entering the lungs. Future studies are needed to evaluate aerosol depositional losses in the delivery system and patient interface, and to develop an aerosol generation system that can provide intermittent submicrometer droplets during NIV. Studies are also needed to assess the continuing growth and deposition of the aerosol as it passes through the tracheobronchial and alveolar airways. Sensitivity analyses are needed to assess the effects of intersubject variability, flow rates, and initial aerosol conditions to optimize delivery for a range of NIV platforms. Ultimately, this approach is envisioned to increase lung aerosol delivery and deposition rates during NIV from the current standard of less than 10% to values of 90% or greater. The ECG approach could also allow the nasal airways to become a preferred aerosol delivery route for pulmonary medicines that require long generation times or frequent applications, which is more convenient and better tolerated than oral inhalation.

Acknowledgments

This study was supported by Award Number R21HL094991 from the National Heart, Lung, And Blood Institute. The content is solely the responsibility of the authors and does not necessarily represent the official views of the National Heart, Lung, And Blood Institute or the National Institutes of Health.

Dr. Jinxiang Xi (University of Arkansas, Little Rock) is gratefully acknowledged and credited for constructing the original version of the NMT geometry used in this study during his time at VCU.

Author Disclosure Statement

The authors declare that no conflicts of interest exist.

References

1. Keenan SP, Kernerman PD, Cook DJ, Martin CM, McCormack D, and Sibbald W: Effect of noninvasive positive pressure ventilation on mortality in patients admitted with acute respiratory failure: a meta-analysis. *Crit Care Med.* 1997;25:1685–1692.
2. Dysart K, Miller TL, Wolfson MR, and Shaffer TH: Research in high flow therapy: mechanisms of action. *Respir Med.* 2009;103:1400–1405.
3. Hess DR: The mask of noninvasive ventilation: principles of design and effects on aerosol delivery. *J Aerosol Med.* 2007;20: S85–S99.
4. Keenan SP, Sinuff T, Cook DJ, and Hill NS: Which patients with acute exacerbation of chronic obstructive pulmonary disease benefit from noninvasive positive-pressure ventilation? A systematic review of the literature. *Ann Intern Med.* 2003;138:861–870.
5. Lightowler JV, Wedzicha JA, Elliott MW, and Ram FSF: Non-invasive positive pressure ventilation to treat respiratory failure resulting from exacerbations of chronic obstructive pulmonary disease: Cochrane systematic review and meta-analysis. *Br Med J.* 2003;326:185–187.
6. Peter JV, Moran JL, Phillips-Hughes J, and Warn D: Noninvasive ventilation in acute respiratory failure—A meta-analysis update. *Crit Care Med.* 2002;30:555–562.
7. Morley CJ, Davis PG, Doyle LW, Brion LP, Hascoet JM, and Carlin JB: Nasal CPAP or intubation at birth for very preterm infants. *N Engl J Med.* 2008;358:700–708.

8. Dewan NA, and Bell CW: Effect of low flow and high flow oxygen delivery on exercise tolerance and sensation of dyspnea. A study comparing the transtracheal catheter and nasal prongs. *Chest*. 1994;105:1061–1065.
9. Chatila W, Nugent T, Vance G, Gaughan J, and Criner GJ: The effects of high-flow vs. low-flow oxygen on exercise in advanced obstructive airways disease. *Chest*. 2004;126:1108–1115.
10. Rea H, McAuley S, Jayaram L, Garrett J, Hockey H, Storey L, O'Donnell G, Haru L, Payton M, and O'Donnell K: The clinical utility of long-term humidification therapy in chronic airway disease. *Respir Med.* 2010;104:525–533.
11. Aboussouan LS and Ricaurte B: Noninvasive positive pressure ventilation: increasing use in acute care. *Clev Clin J Med.* 2010;77:307–316.
12. Ram FS, Lightowler JV, and Wedzicha JA: Non-invasive positive pressure ventilation for treatment of respiratory failure due to exacerbations of chronic obstructive pulmonary disease. *Cochrane Database Syst Rev*. 2004;1:CD004104.
13. Demoule A, Girou E, Richard J-C, Taille S, and Bronchard L: Increased use of noninvasive ventilation in French intensive care units. *Intensive Care Med.* 2006;32:1747–1755.
14. Osthoff M and Leuppi JD: Management of chronic obstructive pulmonary disease patients after hospitalization for acute exacerbation. *Respiration*. 2010;57:255–261.
15. Dhand R: Inhalation therapy in invasive and noninvasive mechanical ventilation. *Curr Opin Crit Care*. 2007;13:27–38.
16. Bhashyam AR, Wolf MT, Marcinkowski AL, Saville A, Thomas K, Carcillo JA, and Corcoran TE: Aerosol delivery through nasal cannulas: an in vitro study. *J Aerosol Med Pulmonary Drug Deliv*. 2008;21:181–187.
17. Shenfield GM, Evans ME, Walker SR, and Paterson JW: Fate of nebulized salbutamol (albuterol) administered by intermittent positive pressure respiration to asthmatic-patients. *Am Rev Respir Dis.* 1973;108:501–512.
18. Dolovich MB, Killian D, Wolff RK, Obminski G, and Newhouse MT: Pulmonary aerosol deposition in chronic-bronchitis—intermittent positive pressure breathing versus quiet breathing. *Am Rev of Respir Dis*. 1977;115:397–402.
19. Parkes SN, and Bersten AD: Aerosol kinetics and bronchodilator efficacy during continuous positive airway pressure delivered by face mask. *Thorax*. 1997;52:171–175.
20. Pollack CV, Fleisch KB, and Dowsey K: Treatment of acute bronchospasm with beta-adrenergic agonist aerosols delivered by a nasal bilevel positive airway pressure circuit. *Ann Emerg Med.* 1995;26:552–557.
21. Nava S, Karakurt S, Rampulla C, Braschi A, and Fanfulla F: Salbutamol delivery during non-invasive mechanical ventilation in patients with chronic obstructive pulmonary disease: a randomized, controlled study. *Intensive Care Med.* 2001;27:1627–1635.
22. Fink JB: Aerosol delivery to ventilated infant and pediatric patients. *Respir Care*. 2004;49:653–665.
23. Bisquerra RA, Botz GH, and Nates JL: Ipratropium-bromide-induced acute anisocoria in the intensive care setting due to ill-fitting face masks. *Respir Care*. 2005;50:1662–1664.
24. Iosson N: Images in clinical medicine: nebulizer-associated anisocoria. *N Engl J Med*. 2006;354:E8.
25. Chatmongkolchart S, Schettino GPP, Dillman C, Kacmarek RM, and Hess DR: In vitro evaluation of aerosol bronchodilator delivery during noninvasive positive pressure ventilation: effect of ventilator settings and nebulizer position. *Crit Care Med.* 2002;30:2515–2519.
26. Branconnier MP, and Hess DR: Albuterol delivery during noninvasive ventilation. *Respir Care*. 2005;50:1649–1653.
27. Sangwan S, Gurses BK, and Smaldone GC: Facemasks and facial deposition of aerosols. *Pediatr Pulmonol*. 2004;37:447–452.
28. Cheng YS: Aerosol deposition in the extrathoracic region. *Aerosol Sci Technol*. 2003;37:659–671.
29. Kelly JT, Asgharian B, Kimbell JS, and Wong B: Particle deposition in human nasal airway replicas manufactured by different methods. Part I: Inertial regime particles. *Aerosol Sci Technol* 2004;38:1063–1071.
30. Dhand R: Aerosol delivery during mechanical ventilation: from basic techniques to new devices. *J Aerosol Med Pulmon Drug Deliv*. 2008;21:45–60.
31. Borgstrom L, Olsson B, and Thorsson L: Degree of throat deposition can explain the variability in lung deposition of inhaled drugs. *J Aerosol Med*. 2006;19:473–483.
32. Longest PW, and Hindle M: CFD simulations of enhanced condensational growth (ECG) applied to respiratory drug delivery with comparisons to in vitro data. *J Aerosol Sci*. 2010;41:805–820.
33. Longest PW, Hindle M, and Xi J: Effective delivery of nanoparticles and micrometer-sized pharmaceutical aerosols to the lung through enhanced condensational growth. International Patent Application PCT/US2009/034360; 2009.
34. Longest PW, McLeskey JT, and Hindle M: Characterization of nanoaerosol size change during enhanced condensational growth. *Aerosol Sci Technol*. 2010;44:473–483.
35. Hindle M, and Longest PW: Evaluation of enhanced condensational growth (ECG) for controlled respiratory drug delivery in a mouth–throat and upper tracheobronchia model. *Pharmaceut Res*. 2010;27:1800–1811.
36. Cox KA, Nguyen TT, McRae DD, Demian BA, and Gregory SM: Condensational aerosols: a new option for targeted delivery of drugs to the pulmonary region. *Respir Drug Deliv* 2002;VIII:231–238.
37. Longest PW, and Xi J: Condensational growth may contribute to the enhanced deposition of cigarette smoke particles in the upper respiratory tract. *Aerosol Sci Technol*. 2008;42:579–602.
38. Ferron GA, Oberdorster G, and Hennenberg R: Estimation of the deposition of aerosolised drugs in the human respiratory tract due to hygroscopic growth. *J Aerosol Med*. 1989;2:271.
39. Hindle M, Byron PR, Jashnani RN, Howell TM, and Cox KA: High efficiency fine particle generation using novel condensation technology. In: RN Dalby, PR Byron, and SJ Farr (eds.). *Proceedings of Respiratory Drug Delivery VI.* Interpharm Press, Inc., Buffalo Grove, IL, pp. 97–102, 1998.
40. Longest PW, and Xi J: Computational investigation of particle inertia effects on submicron aerosol deposition in the respiratory tract. *J Aerosol Sci*. 2007;38:111–130.
41. Xi J, and Longest PW: Numerical predictions of submicrometer aerosol deposition in the nasal cavity using a novel drift flux approach. *Int J Heat Mass Transfer*. 2008;51:5562–5577.
42. Xi J, and Longest PW: Characterization of submicrometer aerosol deposition in extrathoracic airways during nasal exhalation. *Aerosol Sci Technol*. 2009;43:808–827.
43. Guilmette RA, Wicks JD, and Wolff RK: Morphometry of human nasal airways in vivo using magnetic resonance imaging. *J Aerosol Med*. 1989;2:365–377.
44. Guilmette RA, Cheng YS, Yeh HC, and Swift DL: Deposition of 0.005-12 micrometer monodisperse particles in a

computer-milled, MRI-based nasal airway replica. *Inhalat Toxicol*. 1994;6(Suppl. 1):395–399.
45. Kelly JT, Asgharian B, Kimbell JS, and Wong B: Particle deposition in human nasal airway replicas manufactured by different methods. Part II: ultrafine particles. *Aerosol Sci Technol*. 2004;38:1072–1079.
46. Cheng KH, Cheng YS, Yeh HC, and Swift DL: Deposition of ultrafine aerosols in the head airways during natural breathing and during simulated breath-holding using replicate human upper airway casts. *Aerosol Sci Technol*. 1995;23:465–474.
47. Schroeter JD, Kimbell JS, and Asgharian B: Analysis of particle deposition in the turbinate and olfactory regions using a human nasal computational fluid dynamics model. *J Aerosol Med*. 2006;19:301–313.
48. Shi H, Kleinstreuer C, and Zhang Z: Laminar airflow and nanoparticle or vapor deposition in a human nasal cavity model. *J Biomech Eng*. 2006;128:697–706.
49. Segal RA, Kepler GM, and Kimbell JS: Effects of differences in nasal anatomy of airflow distribution: a comparison fo four individuals at rest. *Ann Biomed Eng*. 2008;36:1870–1882.
50. Guilmette RA, Cheng YS, and Griffith WC: Characterising the variabiity in adult human nasal airway dimensions. *Ann Occup Hyg*. 1997;41(Suppl 1):491–496.
51. Guilherme JM, Tewksbury EW, Wong BA, and Kimbell JS: Interindividual variability in nasal filtration as a function of nasal cavity geometry. *J Aerosol Med Pulmon Drug Deliv*. 2009;22:1–17.
52. Xi J, and Longest PW: Transport and deposition of micro-aerosols in realistic and simplified models of the oral airway. *Ann Biomed Eng*. 2007;35:560–581.
53. Longest PW, and Vinchurkar S: Validating CFD predictions of respiratory aerosol deposition: effects of upstream transition and turbulence. *J Biomech*. 2007;40:305–316.
54. Xi J, Longest PW, and Martonen TB: Effects of the laryngeal jet on nano- and microparticle transport and deposition in an approximate model of the upper tracheobronchial airways. *J Appl Physiol*. 2008;104:1761–1777.
55. Longest PW, Hindle M, Das Choudhuri S, and Byron PR: Numerical simulations of capillary aerosol generation: CFD model development and comparisons with experimental data. *Aerosol Sci Technol*. 2007;41:952–973.
56. Matida EA, Finlay WH, and Grgic LB: Improved numerical simulation of aerosol deposition in an idealized mouth–throat. *J Aerosol Sci*. 2004;35:1–19.
57. Longest PW, and Xi J: Effectiveness of direct Lagrangian tracking models for simulating nanoparticle deposition in the upper airways. *Aerosol Sci Technol*. 2007;41:380–397.
58. Longest PW, and Kleinstreuer C: Computational models for simulating multicomponent aerosol evaporation in the upper respiratory airways. *Aerosol Sci Technol*. 2005;39:124–138.
59. Longest PW, and Hindle M: Evaluation of the Respimat Soft Mist inhaler using a concurrent CFD and in vitro approach. *J Aerosol Med Pulmon Drug Deliv*. 2009;22:99–112.
60. Longest PW, Hindle M, and Das Choudhuri S: Effects of generation time on spray aerosol transport and deposition in models of the mouth–throat geometry. *J Aerosol Med Pulmon Drug Deliv*. 2009;22:67–84.
61. Finlay WH: *The Mechanics of Inhaled Pharmaceutical Aerosols*. Academic Press, San Diego; 2001.
62. Hinds WC: *Aerosol Technology: Properties, Behavior, and Measurement of Airborne Particles*. John Wiley and Sons, New York; 1999.
63. Longest PW, and Hindle M: Excipient enhanced growth (EEG) of nanoparticle aerosols to enable improved pulmonary targeting and retention. Provisional Patent Application; 2009.
64. Hering S, and Stolzenburg MR: A method for particle size amplification by water condensation in a laminar, thermally diffusive flow. *Aerosol Sci Technol*. 2005;39:428–436.
65. Ferron GA, Haider B, and Kreyling WG: Conditions for measuring supersaturation in the human lung using aerosols. *J Aerosol Sci*. 1984;15:211–215.
66. Zhang Z, Kleinstreuer C, and Kim CS: Water vapor transport and its effects on the deposition of hygroscopic droplets in a human upper airway model. *Aerosol Sci Technol*. 2006;40:52–67.
67. Shi H, Kleinstreuer C, and Zhang Z: Modeling of inertial particle transport and deposition in human nasal cavities with wall roughness. *J Aerosol Sci*. 2007;38:398–419.
68. Vinchurkar S, Longest PW, and Peart J: CFD simulations of the Andersen cascade impactor: model development and effects of aerosol charge. *J Aerosol Sci*. 2009;40:807–822.

Received on July 27, 2010
in final form, October 25, 2010

Reviewed by:
Jeffry Schroeter
Warren Finlay
Edgar Matida

Address correspondence to:
P. Worth Longest, Ph.D.
Virginia Commonwealth University
P.O. Box 843015
Richmond, VA 23284-3015

E-mail: pwlongest@vcu.edu